Chinese Chemical Letters 35 (2024) 108323

Contents lists available at ScienceDirect

Chinese Chemical Letters

journal homepage: www.elsevier.com/locate/cclet

Probing mitochondrial damage using a fluorescent probe with mitochondria-to-nucleolus translocation

Chi Li[a], Chong Zong[a], Yang Liu[a,b], Zhiqiang Liu[a,b,*], Kang-Nan Wang[a,b,*], Xiaoqiang Yu[a,*]

[a] State Key Laboratory of Crystal Materials, Shandong University, Ji'nan 250100, China
[b] Shenzhen Research Institute of Shandong University, Shenzhen 518057, China

ARTICLE INFO

Article history:
Received 2 December 2022
Revised 5 March 2023
Accepted 8 March 2023
Available online 12 March 2023

Keywords:
Fluorescent probe
Mitochondria targeting
Nucleolus translocation
Mitochondrial damage diagnosis
Fluorescence imaging

ABSTRACT

Mitochondrial damage is closely related to the occurrence of many diseases. However, accurate monitoring and reporting of mitochondrial damage are not easy. Here, we developed a small molecule fluorescent probe named CB-Cl, which has splendid spectral properties (large Stokes shift, strong affinity for RNA, *etc*.) and excellent targeting ability to intracellular mitochondria. After mitochondria were damaged by external stimuli, CB-Cl would light up the nucleolus as a signal reporter. The cascade imaging of mitochondria and nucleolus using CB-Cl can monitor and visualize the mitochondrial status in living cells in real-time. Based on the above advantages, the probe CB-Cl has reference significance for the related research of mitochondrial damage and the prevention and treatment of related diseases.

Mitochondria are essential organelles in eukaryotic cells, known as "cell power factories", which play an important role in energy metabolism and signal transmission of cells [1–3]. Mitochondria provide the vast majority of adenosine triphosphate (ATP) through oxidative phosphorylation (OXPHOS) [4], store metabolites (calcium, iron, lipids and protons, *etc.*), biosynthesize active compounds (iron-sulfur clusters), and act as "gatekeepers" of apoptotic and inflammatory pathways [5]. When mitochondria generate energy, they store electrochemical potential energy in the inner membrane of mitochondria. On both sides of the inner membrane, the asymmetric distribution of proton and other ion concentrations makes mitochondria form a negative transmembrane potential as high as −180 mV, namely the mitochondrial membrane potential (MMP) [6,7]. Hypoxia, drug damage or other stress stimuli may lead to decreased MMP and further dysfunction and oxidative damage, thereby inducing various pathological processes, such as Alzheimer's disease and myocardial injury [8,9]. Therefore, real-time monitoring of mitochondrial status is of great significance for the diagnosis and treatment of related diseases.

Many techniques have been developed to detect mitochondrial damage, including electron probe microscopy (EPM), transmission electron microscopy (TEM) and electrochemical luminescence technology (ECL), *etc*. [10,11]. But these techniques cannot track the dynamics of mitochondria in living cells in real-time. Because of its high specificity, high sensitivity, high contrast and imaging visualization, fluorescence imaging has attracted extensive attention in chemical biology, biochemistry, medicine and other disciplines. Small molecule fluorescent probes based on fluorescence imaging have the advantages of *in situ* and real-time visualization of living cells, low damage to biological samples, and allowing dynamic analysis of living samples. They have also been widely used in subcellular organelle imaging, intracellular biological signal molecule tracking, and marker monitoring of cancer and other diseases [12–17]. At present, JC-1 and other commercial fluorescent dyes developed based on the characteristics of MMP, and some recently reported small molecule fluorescent probes can be used for mitochondrial membrane tracking through J-aggregation and other luminescence methods [18–20]. For example, our group recently developed two fluorescent probes ECPI-12 and IVPI-12, that can image and track the dynamic changes of mitochondria, becoming a potential tool for monitoring and tracking the dynamic changes of mitochondria in living cells and tissues [21]. Li *et al.* developed a vibration-induced-emission based mitochondria targeting fluorescent probe, providing an effective way to detect changes in mitochondrial viscosity [22]. Miller *et al.* developed a fluorescent $\Delta\Psi$m reporter that does not rely on $\Delta\Psi$m-dependent accumulation, which is vital for detecting changes in mitochondrial membrane potential [23]. Although this kind of small molecule fluorescent probes can realize real-time tracking of MMP changes and mitochondrial damage, the narrow Stokes shift of such fluorescent probes and the interference caused by the autofluorescence

* Corresponding authors at: State Key Laboratory of Crystal Materials, Shandong University, Ji'nan 250100, China.
E-mail addresses: zqliu@sdu.edu.cn (Z. Liu), wangkn@sdu.edu.cn (K.-N. Wang), yuxq@sdu.edu.cn (X. Yu).

https://doi.org/10.1016/j.cclet.2023.108323
1001-8417/

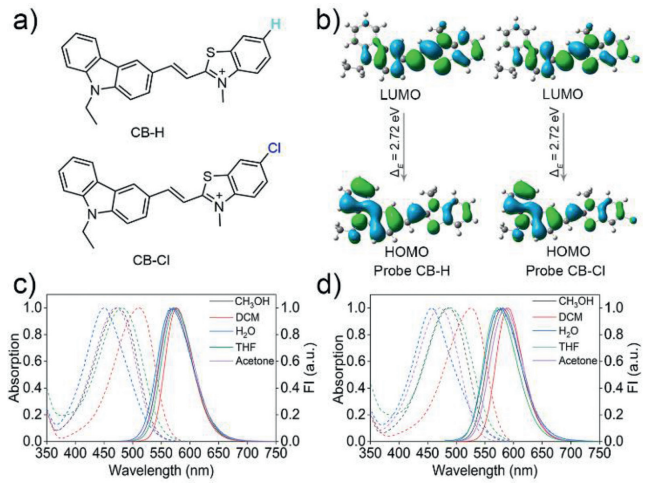

Fig. 1. (a) The structures of probe CB-H and CB-Cl; (b) The frontier orbitals of CB-H and CB-Cl; (c, d) The absorption and fluorescence spectra of CB-H (c) and CB-Cl (d) (10 μmol/L) in different polarity solvents, $\lambda_{ex} = 470$ nm.

of biological macromolecules may lead to problems such as low detection sensitivity and fluorescence crosstalk *in situ* detection. Therefore, it is particularly important to develop novel methods for tracking mitochondrial dynamic changes based on fluorescence imaging.

In order to avoid the fluorescence crosstalk, fluorescent probes with subcellular migratory properties have received increasing attention from researchers. Under normal conditions, the probe can selectively target to a specific subcellular organelle; when the cells are disturbed by external stimuli, the probe would be transferred to other organelles, due to the reduced binding force with this subcellular organelle. Therefore, by tracking the transfer of the probe between the subcellular organelles, the state of the original targeted subcellular organelles can be reflected. Recently, Tang *et al.* developed a fluorescent probe TPE-4EP$^+$, which can translate from mitochondria to nucleus during apoptosis, and real-time monitoring of cell status by fluorescence migration [24]. Mao and Liu *et al.* have developed a cell membrane probe that acts as a signal reporter to illuminate the nucleus once the cell membrane is damaged, which opens up a new avenue for designing membrane damage diagnosis probes for biomedical applications [25]. Although this kind of probe for subcellular organelle migration has made remarkable achievements in monitoring subcellular organelle status, the subcellular migratory probe is still rare, which is challenging to meet the application requirements of medical staff and scientific researchers. Therefore, it is an urgent task to develop fluorescent probes with subcellular migration properties to detect mitochondrial damage.

Fluorescent molecules with D-π-A configuration are one of the primary strategies in designing subcellular organelle targeting probes. Small molecule structures with positive charge can be enriched into mitochondria, nucleus, and other sub-organelles by electrostatic action [26–29]. The benzothiazolium salts are not only a class of electron-absorbing units, but also have been reported to have good nuclear targeting ability. Carbazole and its derivatives are a class of classical electronic donor units [30]. Therefore, fluorescent probe with nucleic acid response and mitochondria/nuclear targeting can be designed by linking benzothiazolium salt and carbazole derivative through conjugated double bonds, which has been confirmed by a reported probe (Fig. 1a) [31]. Herein, a fluorescent probe, CB-Cl, was engineered from the reported probe CB-H, which replaced the hydrogen at the 5-position of benzothiazole monocyclic ring in CB-H with a chlorine atom. Probe CB-Cl is mainly enriched in mitochondria, and when mitochondria are stimulated and the membrane potential decreases, CB-Cl will gradually transfer from mitochondria to the nucleus and further light up nucleoli. This subcellular organelle transfer strategy of mitochondrial escape and nucleolus lighting could be used to reflect the state of mitochondria.

The synthesis path of CB-Cl and CB-H is similar, and the specific synthesis routes are shown in Scheme S1 (Supporting information). The structures were confirmed by ^{1}H NMR, ^{13}C NMR and high resolution mass spectrometry (HRMS) (Figs. S18–S23 in Supporting information). According to the calculation of highest occupied orbital (HOMO) and lowest vacant molecular orbital (LUMO) orbitals of the two molecules by Gaussian 09 (Fig. 1b), the HOMO of the two probes is mainly distributed on *N*-ethyl carbazole, while the LUMO is mainly distributed on benzothiazole unit. This result indicates that a charge transfer process from the *N*-ethylcarbazole to the benzothiazole moiety may have occurred in the two molecules due to their typical D-π-A structural features. The absorption and emission spectra of the two probes in different solvents are shown in Figs. 1c and d, and Tables S1 and S2 (Supporting information). The spectral characteristics of the two probes are similar, and both show polarity dependent spectral changes [32]. In dichloromethane (DCM), significantly red-shifted absorption peaks were detected, which may be due to the formation of halogen bonds [33]. The maximum absorption peak of CB-Cl in water is 457 nm, with a maximum emission peak of 578 nm, such large Stokes shift (~121 nm) can greatly reduce the self-absorption and avoiding the interference of the incident light. Moreover, the red emission of CB-Cl can avoid interference from endogenous fluorophores during bioimaging applications [34].

Then we examined the interaction forms between the probes and nucleic acids in the Tris-HCl buffer. The ultraviolet and visible spectrophotometry (UV–vis) absorption and fluorescence spectra show that the probes exhibit a significant spectral response to nucleic acids and increase in fluorescence as the nucleic acid concentration increases from 0 to 2 mg/mL (Figs. 2a–d, Figs. S1 and S2 in Supporting information). The binding constant (K_a) of probes and DNA were calculated as 2.84×10^6 L/mol and 2.33×10^6 L/mol for CB-Cl and CB-H, respectively (Fig. S3 in Supporting information); and the K_a of probes and RNA were calculated as 3.73×10^6 L/mol and 3.02×10^6 L/mol for CB-Cl and CB-H, respectively, indicating the probe's good affinity to RNA. At the same time, with the increase of probes concentration from 1 μmol/L to 64 μmol/L, the absorption intensity of CB-Cl and CB-H increase gradually with a good linear relationship (Fig. 2e and Fig. S4 in Supporting information), indicating the probes will not aggregate in water, thus eliminating the interference of aggregation at the working concentration of 5–20 μmol/L. In addition, different ratios of methanol-glycerol mixed solution systems were adopted to verify the fluorescence emission characteristics of the probes in viscous environments (Fig. 2f and Fig. S5 in Supporting information) [35]. The significantly enhanced fluorescence in glycerol lays the groundwork for lighting up the highly viscous organelles [36,37]. In order to exclude the influence of pH and various biomolecular species, we conducted different biomolecular species selectivity and pH response experiments on CB-Cl and CB-H (Figs. 2g and h, Fig. S6 in Supporting information). The results show that the change of fluorescence intensity is almost independent of biomolecular species and pH value, which lay a foundation for its application in bioimaging.

In order to further prove the affinity of probe for nucleic acids, AutoDock 4.2 software was adopted for simulation docking study [38]. The binding energies between CB-H and CB-Cl and nucleic acid are shown in Tables S3–S6 (Supporting information). As can be seen, the minimum docking energy to RNA are −29.04 kJ/mol for CB-Cl, and −29.29 kJ/mol for CB-H. In contrast, the lowest binding energies for CB-Cl and CB-H to DNA are −13.89 kJ/mol and

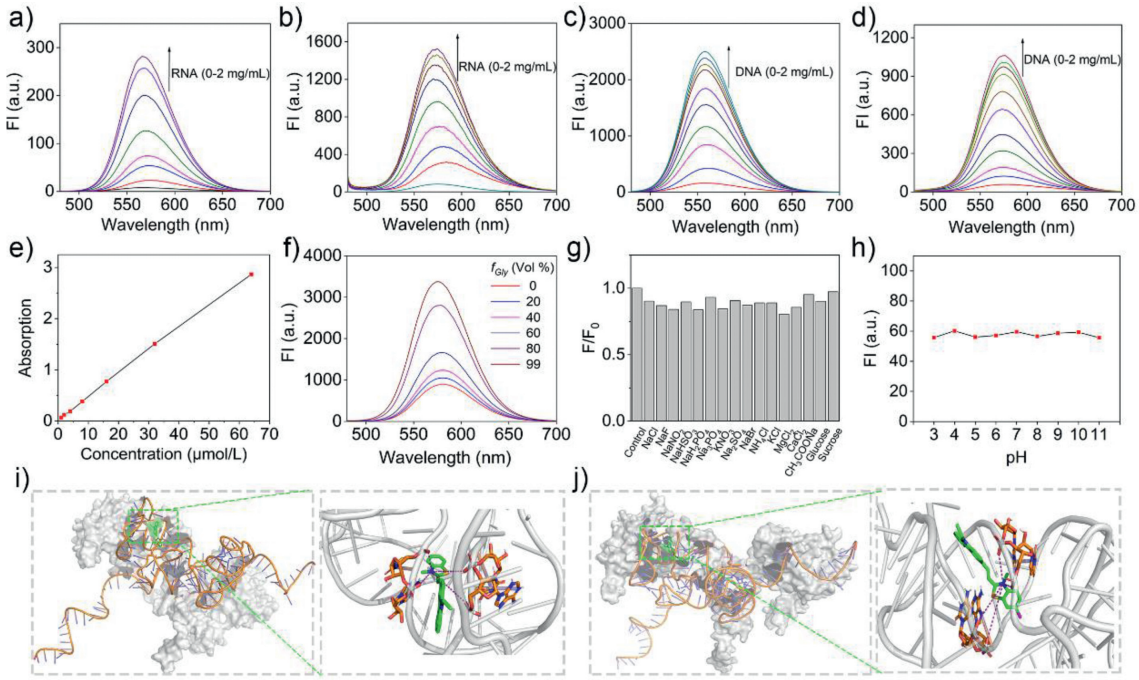

Fig. 2. Emission spectra of CB-H (a, c) and CB-Cl (b, d) (10 μmol/L) in the presence of different concentrations of RNA or DNA in Tris-HCl buffer solution (pH 7.2); (e) Concentration-dependent absorption of CB-Cl in aqueous solution; (f) Emission of CB-Cl (10 μmol/L) in glycerol (Gly)-methanol mixtures at room temperature; (g, h) Fluorescence intensity change of CB-Cl in the presence of different biomolecular species (g) and different pH buffer solutions (h); (i, j) The molecular docking calculations based on the structure optimized CB-H (i) and CB-Cl (j) with RNA secondary structure fragments (PDB No. 5T2C). λ_{ex} = 470 nm.

−13.23 kJ/mol respectively, which means that the probes will preferentially bind to RNA once it encounters nucleic acids. In addition, among the 50 calculated docking genetic algorithm runs of probe and RNA, the number of binding configurations between probes and RNA up to 24, indicate that the probes and RNA have high accessibility. Furtherly, the optimal conformation with the minimum binding energy between the probe and nucleic acid was selected for study (Figs. 2i and j, Fig. S7 in Supporting information). It can be found that the probes are inserted into the minor groove of the nucleic acid, with strong electrostatic interaction between the protonated nitrogen atoms on thiazolium salt and the phosphate acyl unit in nucleic acid. These molecular docking results indicate that both probes CB-H and CB-Cl can show strong binding force with nucleic acids (especially RNA), which lays the foundation for the two probes to light up nucleoli in living cells. The cytotoxicity of CB-H and CB-Cl was then evaluated in HeLa cells before being used for living cell imaging (Fig. S8 in Supporting information). According to the standard MTT assay, the probes exhibit good biocompatibility at working concentrations of 1–20 μmol/L. After stained with different concentrations of probe for 30 min, the fluorescence intensity of two probes increased with the increase of concentration (Figs. S9 and S10 in Supporting information). For CB-H, both the nucleolus and the cytoplasm produced red-light emission, which is consistent with the reported data [31]. For CB-Cl, the staining sites in the cells were observed to be granular or filamentous, which is the typical characteristic of mitochondria. However, no obvious fluorescence was detected in the nucleus. The colocalization experiments with commercial dyes showed that the fluorescence of CB-Cl overlain well with the commercial mitochondrial probe Mito Tracker Deep Red (MTDR) with a Pearson's coefficient of 0.85, while the overlap with other dyes were poor, suggesting that CB-Cl has high specificity for mitochondria (Fig. 3).

In addition, time-lapse imaging was performed after the cells were stained with CB-Cl or CB-H (Figs. 4a and b). For CB-Cl, after the cells were stimulated by light irradiation, the mitochondria were damaged and the MMP decreased [39]. CB-Cl escaped

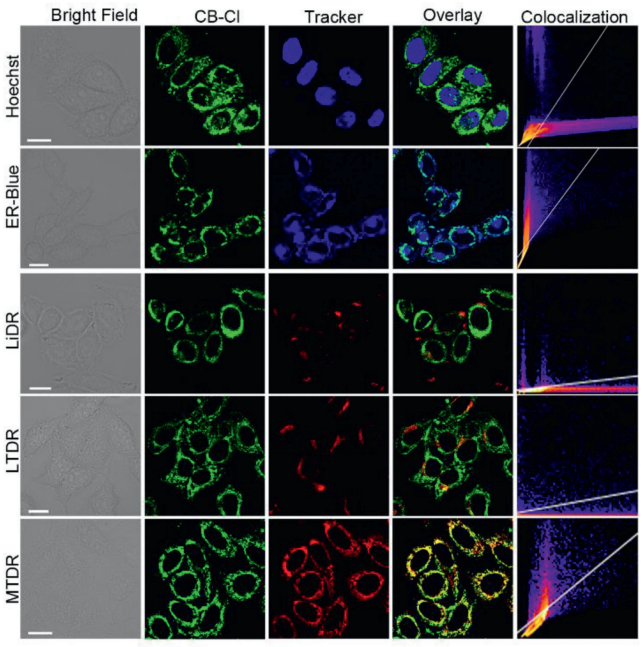

Fig. 3. Fluorescence images of CB-Cl (1 μmol/L) in living HeLa cells. Cells incubated with probe for 30 min and co-stained with different commercial dyes. For CB-Cl, λ_{ex} = 488 nm, λ_{em} = 580–610 nm. For Hoechst 33342, λ_{ex} = 405 nm, λ_{em} = 420–450 nm. For endoplasmic reticulum blue-white DPX (ER-Blue), λ_{ex} = 405 nm, λ_{em} = 460–490 nm. For LiDR, λ_{ex} = 633 nm, λ_{em} = 650–680 nm. For LTDR, λ_{ex} = 633 nm, λ_{em} = 650–680 nm. For MTDR, λ_{ex} = 633 nm, λ_{em} = 650–680 nm. Scale bar: 10 μm.

from mitochondria and bound to RNA in the cytoplasm and nucleolus (Fig. 4c, Movies S1 and S2 in Supporting information). In addition, the dyes outside the cell permeated into cell again, which resulted in increasingly bright fluorescence in the cytoplasm and nucleoli (Fig. 4b). And the time-lapse imaging captured from the

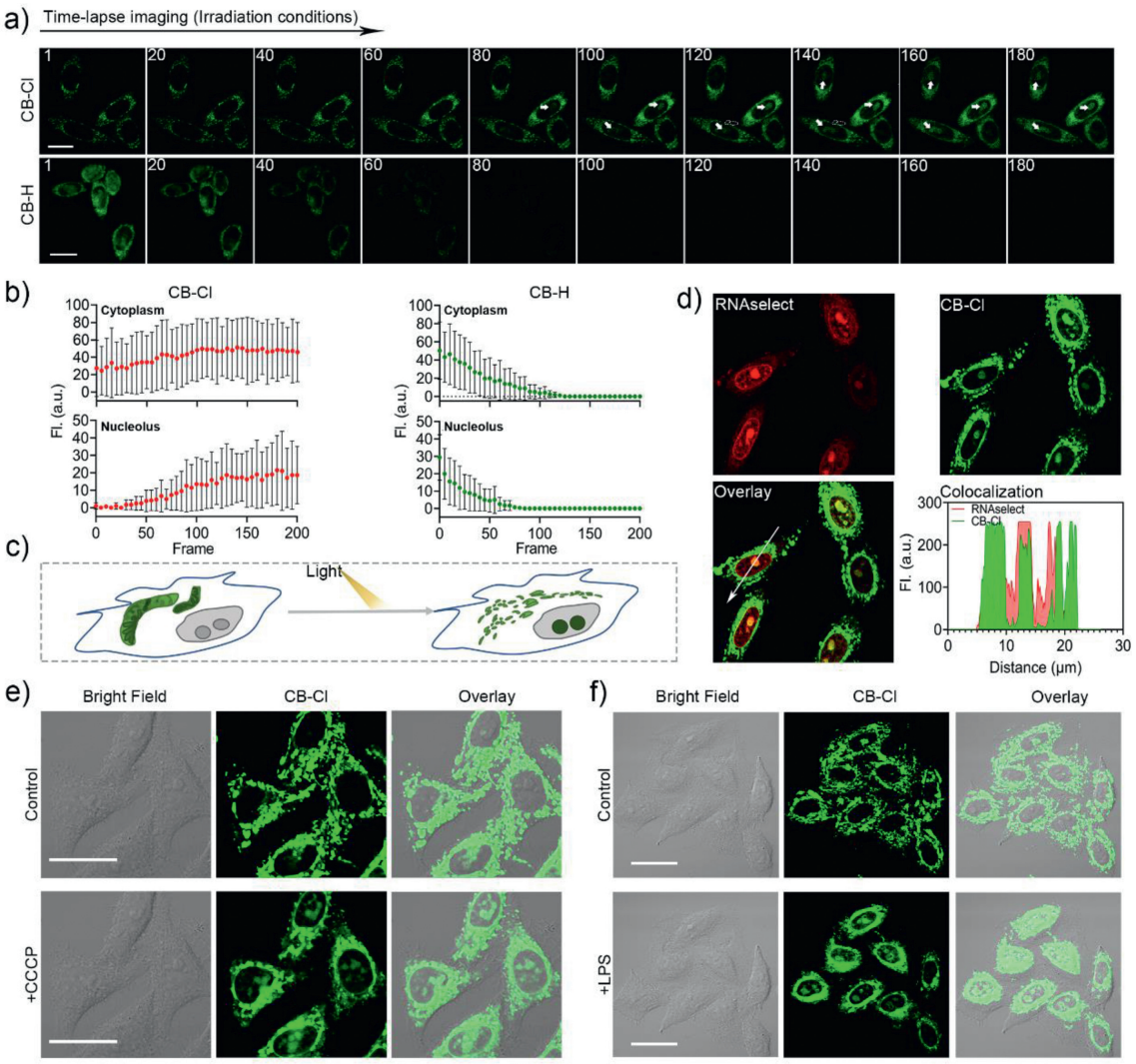

Fig. 4. Fluorescence images of CB-Cl and CB-H in living HeLa cells. (a) Time-lapse imaging of living HeLa cells treated with CB-Cl or CB-H (488 nm, 15 mW/cm^2). The time-dependent fluorescence intensity of living cells after probe treatment was shown in (b). (c) Schematic representation of mitochondria-to-nucleolus translocation of CB-Cl under light-stimulated conditions in living cells. (d) Colocalization of CB-Cl and RNAselect after irradiation. (e, f) Cells were pretreated with CB-Cl (1 μmol/L) for 30 min, then incubated with CCCP (20 μmol/L) (e) or LPS (20 μg/mL) (f) for 15 min (488 nm, 2 mW/cm^2). λ_{ex} = 488 nm, λ_{em} = 580–610 nm. Scale bar: 20 μm.

control group (Fig. S11 in Supporting information) indicated the probe could not enter the nucleolus under dark conditions. And the colocalization experiments with Lidi Deep Red (LiDR) and Lyso Tracker Deep Red (LTDR) after light irradiation showed that CB-Cl may have gone to other organelles after escaping from the mitochondria (Fig. S12 in Supporting information), but this did not affect the nucleolus lighting up. While for CB-H, fluorescence in both cytoplasm and nucleolus was quenched quickly (Movies S3 and S4 in Supporting information), which also reflect the excellent optical stability of CB-Cl. This nucleolar targeting properties of CB-Cl after light exposure was further verified by co-staining with commercial probes RNAselect and Hoechst 33342 (Fig. 4d and Fig. S13 in Supporting information). To evaluate whether the probe CB-Cl can be used to detect the degree of mitochondrial damage in living cells, a model of mitochondria damaging induced by carbonyl cyanide 3-chlorophenylhydrazone (CCCP) was applied (Fig. 4e) [24]. It has been first confirmed that CCCP at the concentration of 20 μmol/L can induce a decrease in MMP without causing cell death (Figs. S14 and S15 in Supporting information). After normal staining with CB-Cl, the cells were treated with CCCP to lose MMP and simulate mitochondria damage. As shown in Fig. 4e, the CCCP-treated mitochondria were progressively broken and fragmented, and the nucleolus in the living cells were light up. Similarly, the same experimental conditions were employed with human astrocytes cells, and similar mitochondrial targeting results were detected (Fig. S16 in Supporting information). After the cells were treated with the inflammation-inducing factor lipopolysaccharide (LPS) for 6 h to induce an inflammatory reaction [40], during this process the mitochondria were also stimulated and damaged. Obviously, the probe also lights up the nucleoli in inflammatory cells (Fig. 4f). While, the living HeLa cells treated with mitochondrial protection drug idebenone (IDBN) [41] could not be detected any fluorescent signal in the nucleolus (Fig. S17 in Supporting information). The mitochondria-nucleolar translocation of CB-Cl results from the changes in mitochondrial damage and decreased MMP, which indicates that it can be used to evaluate mitochondria integrity and MMP changes.

In conclusion, we precisely designed a homologous probe CB-Cl that can migrate from mitochondria to nucleoli after mitochondrial damage. CB-Cl shows a large Stokes shift and high affinity for nucleic acid *in vitro*, and is not responsive to various ions and pH changes. Molecular docking also proves that the probe can produce high binding energy with RNA through electrostatic interaction. Living cell staining show that CB-Cl has a good targeting

effect on mitochondria, and it will be transferred to the nucleoli after mitochondrial damage. These results indicate that the probe can monitor mitochondrial damage by illuminating the nucleolus, which has guiding significance for the design of related probes and the prevention and treatment of mitochondrial related diseases.

Declaration of competing interest

The authors declare that they have no known competing financial interests or personal relationships that could have appeared to influence the work reported in this paper.

Acknowledgments

This work was supported by the Shenzhen Science and Technology Research and Development Funds (No. JCYJ20190806155409104), National Natural Science Foundation of China (Nos. 52150222, 21672130 and 52073163), Guangdong Basic and Applied Basic Research Foundation (No. 2019A1515110356), and the Qilu Young Scholars Program of Shandong University.

Supplementary materials

Supplementary material associated with this article can be found, in the online version, at doi:10.1016/j.cclet.2023.108323.

References

[1] D. Acuna-Castroviejo, M. Martin, M. Macias, et al., J. Pineal Res. 30 (2001) 65–74.
[2] J. Sastre, F.V. Palladó, J. García de la Asunción, J. Viña, Free Radic. Res. 32 (2000) 189–198.
[3] H.M. McBride, M. Neuspiel, S. Wasiak, Curr. Biol. 16 (2006) R551–R560.
[4] M.P. Murphy, Biochem. J. 417 (2009) 1–13.
[5] D.R. Green, G. Kroemer, Science 305 (2004) 626–629.
[6] L.D. Zorova, V.A. Popkov, E.Y. Plotnikov, et al., Anal. Biochem. 552 (2018) 50–59.
[7] L.B. Chen, Ann. Rev. Cell Biol. 4 (1988) 155–181.
[8] A. Logan, I.G. Shabalina, T.A. Prime, et al., Aging Cell 13 (2014) 765–768.
[9] C.A. Galloway, Y. Yoon, Antioxid. Redox Signaling 22 (2015) 1545–1562.
[10] M.R. Angle, A. Wang, A. Thomas, et al., Biophys. J. 107 (2014) 2091–2100.
[11] R. He, H. Tang, D. Jiang, H. Chen, Anal. Chem. 88 (2016) 2006–2009.
[12] A.L. Antaris, H. Chen, K. Cheng, et al., Nat. Mater. 15 (2016) 235–243.
[13] H.M. Kim, B.R. Cho, Chem. Rev. 115 (2015) 5014–5055.
[14] J. Chan, S.C. Dodani, C.J. Chang, Nat. Chem. 4 (2012) 973–984.
[15] L. Gui, K. Wang, Y. Wang, et al., Chin. Chem. Lett. 34 (2023) 107586.
[16] H. Chen, H. Wang, Y. Wei, et al., Chin. Chem. Lett. 33 (2022) 1865–1869.
[17] G. Fang, H. Chen, X. Shao, et al., Small Methods 6 (2022) 2200321.
[18] J. Zhang, Q. Wang, Z. Guo, et al., Adv. Funct. Mater. 29 (2019) 1808153.
[19] Q. Chen, C. Jin, X. Shao, et al., Small 14 (2018) 1802166.
[20] Y. Chen, L.P. Qiao, L.N.A. Ji, H. Chao, Biomaterials 35 (2014) 2–13.
[21] R. Zhang, G. Niu, X. Li, et al., Chem. Sci. 10 (2019) 1994–2000.
[22] S. Wang, B. Zhou, N. Wang, et al., Chin. Chem. Lett. 31 (2020) 2897–2902.
[23] P.E.Z. Klier, J.G. Martin, E.W. Miller, J. Am. Chem. Soc. 143 (2021) 4095–4099.
[24] T. Zhang, Y. Li, Z. Zheng, et al., J. Am. Chem. Soc. 141 (2019) 5612–5616.
[25] K.N. Wang, G.B. Qi, H.Y. Chu, et al., Mater. Horiz. 7 (2020) 3226–3233.
[26] J. Cui, Y. Yao, C. Chen, et al., Chin. Chem. Lett. 30 (2019) 1071–1074.
[27] H. Jiang, G. Yin, Y. Gan, et al., Chin. Chem. Lett. 33 (2022) 1609–1612.
[28] X.C. Chen, S.B. Chen, J. Dai, et al., Angew. Chem. Int. Ed. 57 (2018) 4702–4706.
[29] X. Luo, B. Xue, G. Feng, et al., J. Am. Chem. Soc. 141 (2019) 5182–5191.
[30] N. Koumura, Z.S. Wang, S. Mori, et al., J. Am. Chem. Soc. 128 (2006) 14256–14257.
[31] J.B. Chao, Z.Q. Li, Y.B. Zhang, et al., J. Mater. Chem. B 4 (2016) 3703–3712.
[32] Z.R. Grabowski, K. Rotkiewicz, W. Rettig, Chem. Rev. 103 (2003) 3899–4032.
[33] G. Cavallo, P. Metrangolo, R. Milani, et al., Chem. Rev. 116 (2016) 2478–2601.
[34] C. Ince, J.M. Coremans, H.A. Bruining, Adv. Exp. Med. Biol. 317 (1992) 277–296.
[35] Z.R. Grabowski, K. Rotkiewicz, A. Siemiarczuk, D.J. Cowley, W. Baumann, Nouv. J. Chim. 3 (1979) 443–454.
[36] K. Rotkiewicz, K.H. Grellmann, Z.R. Grabowski, Chem. Phys. Lett. 19 (1973) 315–318.
[37] C.C. Chang, J.F. Chu, H.H. Kuo, et al., J. Lumin. 119 (2006) 84–90.
[38] G.M. Morris, R. Huey, W. Lindstrom, et al., J. Comput. Chem. 30 (2009) 2785–2791.
[39] I. Kim, J.J. Lemasters, Antioxid. Redox Signal. 14 (2010) 1919–1928.
[40] M. Bosch, M. Sánchez-Álvarez, A. Fajardo, et al., Science 370 (2020) eaay8085.
[41] Y. Ikejiri, E. Mori, K. Ishii, et al., Neurology 47 (1996) 583–585.